Micro and Nano Engineering 1 (2018) 37–41

Contents lists available at ScienceDirect

Micro and Nano Engineering

journal homepage: www.elsevier.com/locate/tsf

Regular paper

# Optical properties of shortest-width zig-zag silicene nano-ribbons: Effects of local fields

Matteo Ferri [a,b], Guido Fratesi [b], Giovanni Onida [b], Alberto Debernardi [a,*]

[a] CNR-IMM, sede Agrate Brianza, via Olivetti 2, Agrate Brianza I-20864, Italy
[b] Dipartimento di Fisica and ETSF, Università degli Studi di Milano, via Celoria 16, Milano I-20133, Italy

ARTICLE INFO

*Article history:*
Received 8 May 2018
Received in revised form 6 September 2018
Accepted 12 October 2018

*Keywords:*
Silicene
Optoelectronic properties
First principles simulations
2D materials
Optical spectra
Nanoribbons.

ABSTRACT

We have computed from first principles the structural, magnetic and optical properties of zig-zag oriented silicene nanoribbons. The minimal width for structurally stable planar structure having zig-zag edges corresponds to a 4-chains ribbon. Its ground state presents reconstructed and spin polarized edges, coupled antiferromagnetically. For this state, and for the corresponding excited state with ferromagnetically coupled edges, we computed the optical absorption spectra within the independent particle approximation, including local field effect corrections, for light polarized in the directions parallel and perpendicular to the ribbon axis. For the "parallel" light polarization the inclusion of local fields effects is limited to a slight reduction of the intensity of the main peak in the infrared region, as well as that of some minor peaks in the visible-ultraviolet structure. Conversely, the computed optical spectrum for light polarized perpendicularly to the ribbon axis shows that the short-width zig-zag nanoribbons are basically transparent in the infrared and visible region, because of the effect of electronic confinement combined with local fields.



## 1. Introduction

Silicene, the silicon analogous of graphene, is a honeycomb structure, essentially retaining the two-dimensional (2D) character of graphene, but made by silicon instead of carbon. As a free-standing material, silicene is predicted to display an electronic band-structure characterized by Dirac's cones, being stable in a buckled configuration [1,2]. The practical interest and potential applications of silicene for future electronic devices arose from the well-known limits of the traditional device down-scaling, which has reached the bounds of electrostatics and short-channel effects threatening the continuance of Moore's law. In fact, the electronic industry has already moved to thin film channel devices. Silicene is indeed a promising material to reach the ultimate limit of channel thickness [3].

Further, the prediction of planar pseudomorphic heterostructures based on silicene [4] suggests a new scenario, where ultra-scaled 2D devices can be tailored according to the need of the electronic industry. Silicene can benefit of its compatibility with the current industrial processes based on the silicon technology. The recent experimental measurement of a 2D silicene sheet on metallic substrate [5–9] has triggered further attention on these materials [10–13]. However, the strong coupling between the epitaxial silicene lattice and its metal hosting substrate [14] inhibits the required semiconducting properties and represents a drawback in the fabrication of functional electronic devices.

The opening of an energy gap is also necessary for on/off switching. A possible way to achieve this condition in silicene consists in restricting the geometry into one dimension, by constructing nanoribbons, i.e. silicene stripes of finite width. Ab-initio calculations predicted that free-standing silicene nanoribbons with zig-zag edges have an antiferromagnetic semiconducting ground-state [15], which may find some possible applications in nanoelectronics and spintronics. For this reason, in the present work we limited our study to zig-zag terminated silicene nano-ribbons and evaluate the relaxed geometry, the electronic properties, and the optical absorption spectra of the silicene ribbon with zig-zag edges having the shortest width: the 4-chains zig-zag silicene nanoribbon (4-ZSiNR).

Our paper is organized as follows: in Section 2 we give a brief account of the computational techniques we used. In Section 3 we present the relaxed structure and the electronic properties, and we discuss the effect of spin-orbit coupling on the electronic band-structure in Section 4. In Section 5 we present and discuss our results for the absorption spectra for both light polarization parallel and perpendicular to the

* Corresponding author.
*E-mail address:* alberto.debernardi@mdm.imm.cnr.it (A. Debernardi).

https://doi.org/10.1016/j.mne.2018.10.002

ribbon axis, computed within the independent particle random phase approximation and by including the effects of local fields. Our conclusions are summarized in Section 6.

## 2. Computational methods

The structural and electronic properties of the nanoribbons were computed in the framework of the Density Functional Theory (DFT), using the Quantum Espresso (QE) open-source code [16]. We employed a fully relativistic norm-conserving pseudopotential, generated with the Perdew-Burke-Ernzerhof (PBE) exchange-correlation functional [17] and we expanded the wavefunction in plane waves up to a kinetic energy cutoff of 75 Ry.

We describe the geometric structure of the ribbon with a tetragonal supercell, in which a vacuum region of 15 Å is set in the directions perpendicular to the ribbon axis in order to avoid unphysical interactions between the periodic repeated replicas of the unit cell. The cell was doubled along the ribbon direction, in order to reproduce the $(2 \times 1)$ edge reconstruction reported in the literature [2,15]. The Brillouin Zone (BZ) was sampled with a uniform $45 \times 1 \times 1$ Monkhorst-Pack (MP) [18] grid in the non magnetic (NM) and ferromagnetic (FM) configuration and with a uniform $15 \times 1 \times 1$ MP grid in the antiferromagnetic (AFM) case. The atomic positions and the lattice constant were relaxed using the Broyden-Fletcher-Goldfarb-Shanno (BFGS) algorithm [19] with a threshold on the forces of 0.25 meV/Å.

All the optical spectra calculations were carried out using the YAMBO code [20]. The macroscopic dielectric constant was computed using 236 empty states and a $25 \times 1 \times 1$ MP grid of k-point for the AFM ribbons and a $60 \times 1 \times 1$ for the FM ones. The effect of the local fields has been taken into account with an energy cutoff of 1 Ry and 2 Ry for the FM and the AFM configuration, respectively. Those values differ because the greater number of *k*-points used to sample the BZ of the FM 4-ZSiNR requires more computational resources forcing us to limit the values of the other parameters.

## 3. Structural and electronic properties

In the present work, we consider 4-chains zig-zag silicene nanoribbons (4-ZSiNRs), since this structure corresponds to the minimum width in which silicene is stable in the ribbon geometry with zig-zag edges. In fact, a zig-zag ribbon composed of 3-chains reconstructs in a 1D-wire-like structure, as shown and discussed in the appendix. We constructed 4-chain zig-zag silicene nanoribbons by cutting stripes from the geometric structure of the low-buckled honeycomb silicene as a starting point for structural optimizations.

The relaxed atomic positions of the structure with lower energy is displayed in the top-panel of Fig. 1. The structure presents a triangle-

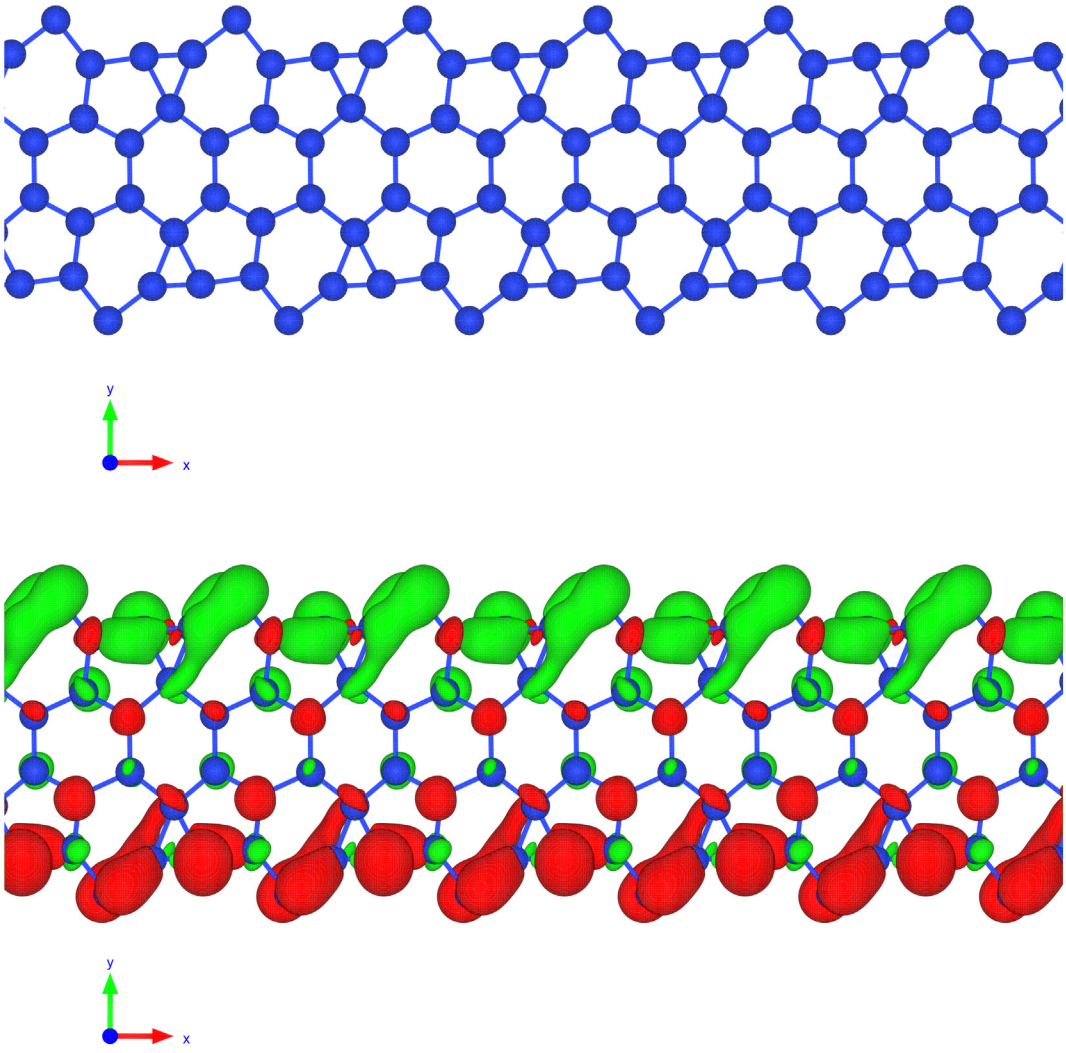


**Fig. 1.** Top panel: the relaxed structure of 4-chains zig-zag silicene nanoribbon having opposite spin-polarization at the edges. Bottom panel: the valence charge density in the opposite spin populations (red, green) showing the isosurfaces corresponding to an electron density of 6% of its maximum value).

pentagon (TP) pair reconstruction at the edges. The lowest-energy state of this structure exhibits a magnetic configuration with opposite spin orientations between the two edges, each of them being ferromagnetically ordered, as shown by the charge density reported in the bottom panel of Fig. 1. We will refer to this structure as the antiferromagnetic (AFM) configuration. This globally AFM structure is a magnetic semiconductor with an indirect bandgap of 0.194 eV, and is the ground state of the system. At variance, if the structural optimization starts with a globally ferromagnetic state (i.e., same spin polarization on both edges), the system relaxes to a local minimum of the energy, slightly higher than the ground state. The corresponding electronic structure for the magnetic configuration with the same spin, i.e. for a globally ferromagnetic (FM) state, shows that the system is a semimetal, as long as the spin-orbit interaction is neglected.

The electronic band-structure for AFM and FM configuration are displayed in Fig. 2. The AFM ribbon is a magnetic semiconductor with indirect bandgap of ≈0.2 eV; its electronic bands are doubly degenerate as an effect of the combination of time reversal and inversion symmetries. The FM ribbon is a magnetic semi-metal with distinct spin up and spin down bands. At the Fermi energy the spin up and spin down bands display a linear dispersion, thus forming the analogous of a Dirac cone, in one dimension.

## 4. Spin-orbit effects on the band structure

We investigated the effect of spin orbit polarization in confined nanostructures. The inclusion of the spin-orbit coupling in the AFM 4-ZSiNR TP structure further lowers the total energy by 0.2 meV per atom but it does not affect the band structure. The bands, shown in the left panel of Fig. 2 remain still double degenerate, since the spin-orbit term, that in atomic physics is proportional to the scalar product between spin ($\vec{S}$) and angular momentum ($\vec{L}$) operators, $\vec{S}\cdot\vec{L}$, is invariant both for time-reversal and for spatial inversion symmetry. As for the AFM structure, for the FM structure we also find a total energy lowering of 0.2 meV per atom due to the inclusion of spin-orbit effects. However, as can be noticed in the right panel of Fig. 2 in this case the inclusion of the spin-orbit coupling also affects the band structure, by opening a small gap of 4.5 meV at the crossing point. This value is higher than the one found in 2D silicene (1.55 meV) [21], due to the larger buckling of edge atoms with respect to the case of an infinite honeycomb silicene layer, induced by a more pronounced $sp^3$ hybridization. The spin-orbit coupling has in fact a greater effect on the $sp^3$ hybridization than on the $sp^2$ one. Indeed, the splitting due to spin-orbit coupling observed in the band-structure of 3D bulk silicon, being totally $sp^3$ hybridized, amounts to the value of 42.6 meV [22].

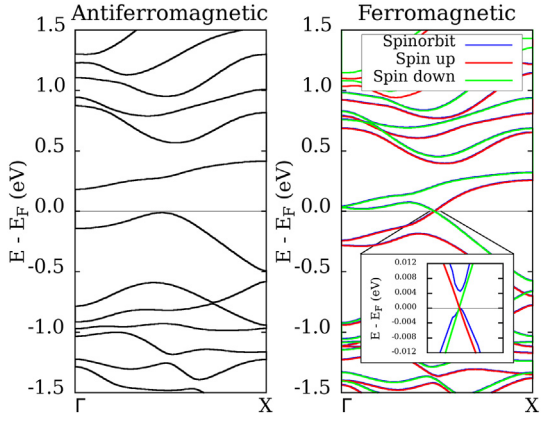


**Fig. 2.** Spin-orbit effect on the band structure of 4-chains zig-zag silicene nanoribbon with anti-ferromagnetic (left panel) and ferromagnetic (right panel) coupling between the edges polarization. Inset: for ferromagnetic coupling, spin-orbit effects open a small band gap of 4.5 meV at the crossing point of spin-up (red solid line) and spin-down (green solid line) bands, computed neglecting spin orbit interaction. The Fermi level is set at the valence band maximum.

## 5. Optical properties

The optical absorption – a property of paramount importance for technological exploitation – is proportional to the imaginary part of the macroscopic dielectric function, $\varepsilon_M(\omega)$. The latter can be obtained from microscopic quantities such as the response function $\chi_{G,G'}(q,\omega)$ [23,24]. Response functions can in turn be computed on the basis of transition matrix elements between electronic states, with the inclusion of both interband and intraband transitions in the case of metals.

In the framework of Many-Body Perturbation Theory, several approximations can be used, corresponding to increasing levels of theoretical refinement, ranging from the simplest approach, i.e. the bare independent particle–random phase approximation (IP-RPA), to more complete approaches where, e.g., local fields and/or excitonic effects are included. In the long wavelength limit, which is appropriate for spectra obtained by Ultraviolet-Visible Spectroscopy (UV-VIS), the macroscopic dielectric function $\varepsilon_M$ can be expressed as:

$$\varepsilon_M(\omega) = \lim_{q\to 0} \frac{1}{\left[\varepsilon^{-1}_{GG'}(q,\omega)\right]_{G=0G'=0'}}, \tag{1}$$

involving only the $G = 0, G' = 0$ "head" of the *appropriate* inverse microscopic dielectric function written in reciprocal space as [23]:

$$\varepsilon^{-1}_{GG'}(q\omega) = \delta_{GG'} + v(q+G)\chi_{GG'}(q\omega) \tag{2}$$

Here, $v$ is the Coulomb potential, $\chi_{GG'}(q\omega)$ is the reducible polarizability, that in the RPA is expressed in terms of the irreducible polarizability as:

$$\chi_{GG'}(q\omega) = \left[\delta_{GG''} - v(q+G'')\chi^0_{GG''}(q\omega)\right]^{-1}\chi^0_{G''G'}(q\omega), \tag{3}$$

where the non–interacting response function $\chi^0_{GG'}(q\omega)$ is constructed from the Kohn-Sham eigenvalues, eigenfunctions, and occupations ($\varepsilon$, $\psi$, and $f$; $V$ is the unit-cell volume):

$$\chi^0_{GG'}(q,\omega) = -\frac{1}{V}\sum_{nk}\sum_{mk'}(f_{nk}-f_{mk'})\left(\frac{\left\langle\psi^{KS}_{mk'}\left|e^{i(q+G)r}\right|\psi^{KS}_{nk}\right\rangle\left\langle\psi^{KS}_{nk}\left|e^{-i(q+G')r'}\right|\psi^{KS}_{mk'}\right\rangle}{\varepsilon^{KS}_{mk'}-\varepsilon^{KS}_{nk}-\omega-i\eta}\right) \tag{4}$$

In this work, we investigate the role played by different approximations, starting from the bare independent-particle (IP) approximation, in which only the $G \neq 0$, $G' \neq 0$ term of the response function from Eq. (3) is taken into account. The local–field (LF) effects are completely neglected within this approximation; they can be included by summing explicitly the $G \neq 0$, $G' \neq 0$ components of the response function in Eq. (2).

### 5.1. Dielectric response of AFM 4-ZSiNR

We report in Fig. 3 the imaginary part of the dielectric function of the AFM 4-ZSiNR, for light polarization parallel to the ribbon axis (Fig. 3(a)) and perpendicular to it (Fig. 3(b)), i.e., for light polarized along the $x$ and $y$ directions marked in Fig. 1. The black dashed lines represent the IP-RPA results, while the green lines represent the RPA ones, in which the local fields are taken into account. An energy cutoff of 2 Ry is used for the G vector contribution in reciprocal space. Note that Fig. 3 (a) and Fig. 3(b) are depicted with the same scale on the vertical axis in order to reveal the polarization dependence in the absorption spectrum. The parallel light polarization absorption spectrum at IP-RPA level is characterized by a main absorption peak at 0.3 eV, which is

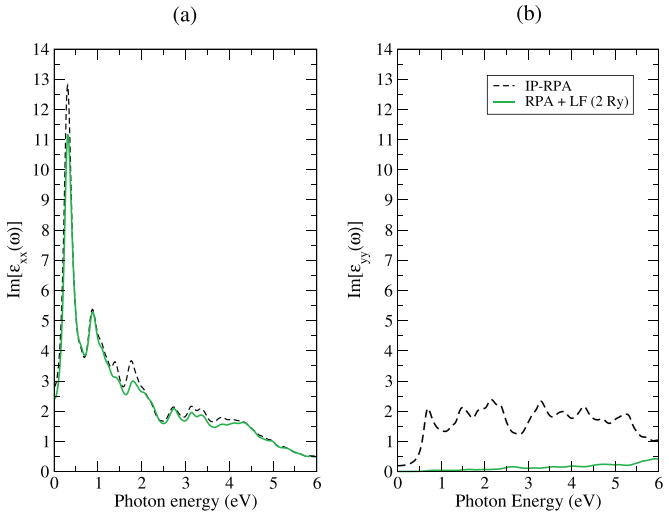


**Fig. 3.** (Absorption spectra) Imaginary part of the dielectric function of the antiferromagnetic 4-ZSiNR in TP configuration, for light polarized along the ribbon axis (a) and perpendicular to it (b). We take into account the local-field (LF) effects with a 2 Ry cutoff radius.

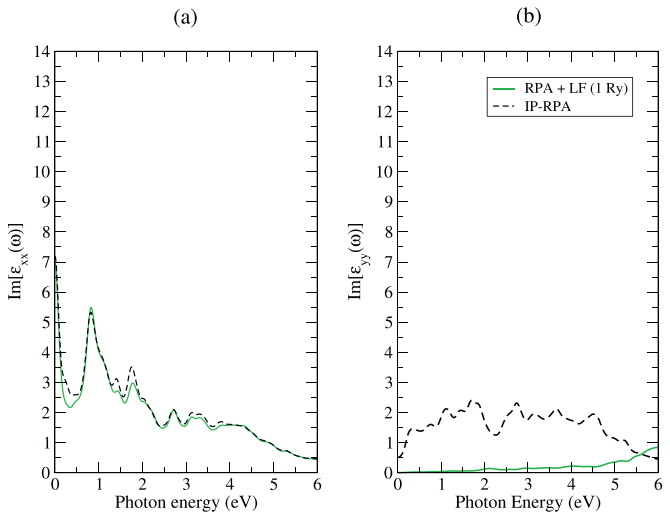


**Fig. 4.** Imaginary part of the dielectric function of the FM 4-ZSiNR in TP configuration, for light polarized along the ribbon axis (a) and perpendicular to it (b). We take into account the local-field (LF) effects with a 1 Ry cutoff radius.

due to the transitions between the highest unoccupied and the lowest unoccupied bands, around the Fermi level, in the first half BZ. There, these two bands run almost parallel, with an energy difference of 0.3 eV, indeed. We notice also a weaker absorption peak at 0.8 eV. The perpendicularly polarized light at IP-RPA level shows some peaks, whose intensity is much smaller than that one of the parallel light polarization.

When the inhomogeneities of the system are taken into account through the inclusion of the local field effects, the spectrum with light polarized in the parallel direction is slightly affected. We notice only a small reduction (15%) in the intensity of the main absorption peak at 0.3 eV and of the peak at 1.8 eV. Conversely, a huge suppression of the intensity occurs in the spectrum of the perpendicular light polarization, making the nanoribbon almost transparent below 5 eV. This strong reduction of the intensity for the perpendicular light polarization is typical of the 1D confined systems. Indeed, it has been found by first principle calculations in silicon [25] and germanium [26] nanowires and experimentally observed in carbon nanotubes [27]. This effect is mainly due to the anisotropies in nanostructured systems.

In anisotropic nano-structures it is important to include the microscopic components generated in response of a macroscopic external field especially in the shortest directions where confinement effects are more important, because the so-called LF or depolarization effects involve local contributions as the induced microscopic variations of the Hartree potential: in our case, LF effects suppress absorption at lower energies when the light polarization is perpendicular to the nanoribbon edges, while small modifications to the spectra are observed for parallel polarization.

### *5.2. Dielectric response of FM 4-ZSiNR*

Let us consider now the FM 4-ZSiNR. We recall that the spin-orbit coupling opens a small gap around the crossing point of spin-up and spin-down band at the Fermi level. Given the smallness of the band gap, and since these states around the Fermi level, being those that mainly contribute to the optical properties at low energy, show a significant dispersion with $k$, we need to use a denser $k$-mesh in order to sample adequately the bands around the gap.

Therefore, after solving the Kohn-Sham equations with a $45 \times 1 \times 1$ $k$-grid, we perform the computation of the wavefunction and the eigenvalues on a $60 \times 1 \times 1$ $k$-grid. The optical response both for parallel and perpendicular light polarization is reported in Fig. 4. Fig. 4 is depicted with the same vertical axis scale of Fig. 3 in order to compare them.

We notice that the main absorption peak of the AFM 4-ZSiNR for the parallel light polarization is converted in a Drude-like peak for small frequencies, which is clearly due to the transitions between states in correspondence of the small energy gap. Apart from the shift of the main peak, the absorption spectrum of the FM 4-ZSiNR resembles the AFM one, showing the same peak at 0.9 eV. The Drude-like peak constitutes the fingerprint of the FM 4-ZSiNR and could be used to distinguish experimentally the two different magnetic configurations.

In Fig. 4(b) we can see that the intensity of the spectrum corresponding to the perpendicular light polarization is suppressed with the inclusion of the local fields effects, due to anisotropies. The lower cutoff energy used for FM 4-ZSiNR than that used for the AFM 4-ZSiNR is already sufficient to suppress the intensity of the perpendicular light polarization, without changing appreciably the one for parallel polarization. Thus, for both antiferromagnetic and ferromagnetic polarization of spin of edges states, in the infra-red and visible range of the spectrum the ribbon is transparent for light polarized perpendicular to its axis, while it absorbs radiation for light polarized parallel to its axis, thus acting as a light polarizer on nanometer length-scale.

## 6. Conclusions

Summarizing, we determined the minimum width at which a silicene zig-zag nanoribbon is structurally stable. We evaluated its electronic structure and the influence of spin-orbit effects that are found to open a band gap in the ferromagnetically coupled configuration. As a preliminary step we computed the absorption spectrum within the bare independent-particle approximation. The inclusion of the local-field effects suppresses the intensity of the absorption spectrum for the light polarization perpendicular to the nanoribbon axis, making the nanoribbon almost transparent, whereas more intense features computed in the dielectric constant for parallel light polarization are preserved. These differences in absorption/transmission of light polarized parallel or perpendicular to the axis of the nanoribbon, make short-width SiNRs promising candidates as absorptive linear polarizers from infrared to ultra-violet frequencies in forthcoming ultra-scaled devices.

## Conflict of Interest

The authors declare that they have no known competing financial interests or personal relationships that could have appeared to influence the work reported in this paper.

## Acknowledgments

We acknowledge the CINECA and the Regione Lombardia award under the LISA initiative (ASSO project), for the availability of high performance computing resources and support, CINECA for computer resources allocated under ISCRA initiative (OPSiN project), and R. Colnaghi for technical support on computer hardware.

## Appendix A. Critical width of zig-zag nanoribbons

We established the critical width $n_c$ below which the zig-zag silicene ribbon is structurally unstable. We found a value of $n_c = 4$, which means that nanoribbons having the size equal or larger than 4-zigzag chains are structurally stable. At variance, the 3-chains zig-zag silicene is found to be unstable in a nanoribbon configuration and it spontaneously reconstructs in a kind of nanowire-like structure, shown in Fig. 5. Its total energy per atom is 0.225 eV lower than the one of the nanoribbon-like configuration, which was the starting point of the Broyden-Fletcher-Goldfarb-Shanno (BFGS) relaxation [19]. Therefore the 4-chain zig-zag silicene nanoribbon (4-ZSiNR) can be considered as the structure with the lowest-width that can be stable in a nanoribbon geometry having zig-zag edge orientation.

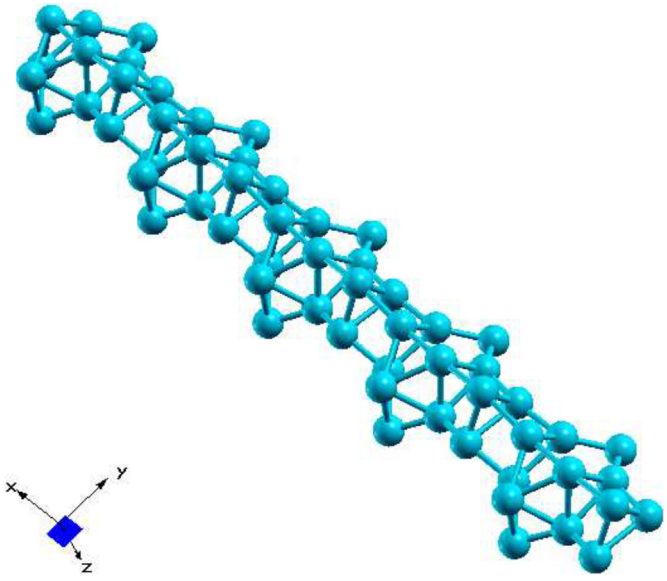


**Fig. 5.** Nanowire-like structure obtained by atomic relaxation of a 3-chains zig-zag nanoribbon of silicene.

## References

[1] K. Takeda, K. Shiraishi, Phys. Rev. B 50 (1994) 14916.
[2] S. Cahangirov, M. Topsakal, E. Aktürk, H. Sahin, S. Ciraci, Phys. Rev. Lett. 102 (2009) 236804.
[3] A. Dimoulas, Microelectron. Eng. 131 (2015) 68–78.
[4] A. Debernardi, L. Marchetti, Phys. Rev. B 93 (2016) 245426.
[5] P. De Padova, C. Quaresima, P. Perfetti, B. Olivieri, C. Leandri, B. Aufray, S. Vizzini, G. Le Lay, Nano Lett. 8 (2008) 271.
[6] P. Vogt, P. De Padova, C. Quaresima, J. Avila, E. Frantzeskakis, M.C. Asensio, A. Resta, B. Ealet, G. Le Lay, Phys. Rev. Lett. 108 (2012) 155501.
[7] A. Fleurence, R. Friedlein, T. Ozaki, H. Kawai, Y. Wang, Y. Yamada-Takamura, Phys. Rev. Lett. 108 (2012) 245501.
[8] L. Meng, Y. Wang, L. Zhang, S. Du, R. Wu, L. Li, Y. Zhang, G. Li, H. Zhou, W.A. Hofer, H.J. Gao, Nano Lett. 13 (2013) 685.
[9] H. Enriquez, A. Kara, A.J. Mayne, G. Dujardin, H. Jamgotchian, B. Aufray, H. Oughaddou, J. Phys. Conf. Ser. 012004 (2014) 491.
[10] S. Cahangirov, M. Audiffred, P. Tang, A. Iacomino, W. Duan, G. Merino, A. Rubio, Phys. Rev. B 88 (2013) 035432.
[11] E. Cinquanta, G. Fratesi, S. Dal Conte, C. Grazianetti, F. Scotognella, S. Stagira, C. Vozzi, G. Onida, A. Molle, Phys. Rev. B 92 (2015) 165427.
[12] P.M. Sheverdyaeva, S.Kr. Mahatha, P. Moras, L. Petaccia, G. Fratesi, G. Onida, C. Carbone, ACS Nano 11 (2017) 975.
[13] L. Tau, E. Cinquanta, D. Chiappe, C. Grazianetti, M. Fanciulli, M. Dubey, A. Molle, D. Akinwande, Nat. Nanotechnol. 10 (2015) 227.
[14] C. Grazianetti, E. Cinquanta, A. Molle, 2D Mater 012001 (2016) 3.
[15] R. Li, J. Zhou, Y. Han, J. Dong, Y. Kawazoe, J. Chem. Phys. 139 (2013) 104703.
[16] P. Giannozzi, S. Baroni, N. Bonini, M. Calandra, R. Car, C. Cavazzoni, D. Ceresoli, G.L. Chiarotti, M. Cococcioni, I. Dabo, A. Dal Corso, S. Fabris, G. Fratesi, S. de Gironcoli, R. Gebauer, U. Gerstmann, C. Gougoussis, A. Kokalj, M. Lazzeri, L. Martin-Samos, N. Marzari, F. Mauri, R. Mazzarello, S. Paolini, A. Pasquarello, L. Paulatto, C. Sbraccia, S. Scandolo, G. Sclauzero, A.P. Seitsonen, A. Smogunov, P. Umari, R.M. Wentzcovitch, J. Phys. Condens. Matter 21 (2009) 395502.
[17] J.P. Perdew, K. Burke, M. Ernzerhof, Phys. Rev. Lett. 77 (1996) 3865.
[18] H.J. Monkhorst, J.D. Pack, Phys. Rev. B 13 (1976) 5188.
[19] C.G. Broyden, IMA J. Appl. Math. 6 (1970) 76.
[20] A. Marini, C. Hogan, M. Grüning, D. Varsano, Comput. Phys. Commun. 180 (2009) 1392.
[21] Cheng-Cheng Liu, Wanxiang Feng, Yugui Yao, Phys. Rev. Lett. 107 (2011) 076802.
[22] Yu Zhiyi, Y.X. Huang, S.C. Shen, Phys. Rev. B 39 (1989) 6287(R).
[23] G. Onida, L. Reining, A. Rubio, Rev. Mod. Phys. 74 (2002) 601.
[24] G. Strinati, Riv. Nuovo Cimento Soc. Ital. Fis. 11 (1988) 1.
[25] F. Bruneval, S. Botti, L. Reining, Phys. Rev. Lett. 94 (2005) 219701.
[26] M. Bruno, M. Palummo, A. Marini, R. Del Sole, V. Olevano, A.N. Kholod, S. Ossicini, Phys. Rev. B 72 (2005) 153310.
[27] N. Wang, Z.K. Tang, G.D. Li, J.S. Chen, Nature 408 (2000) 50.